

The Global Carbon Budget as a cointegrated system*

Mikkel Bennedsen[†], *Eric Hillebrand*[‡], *Morten Ørregaard Nielsen*[§]

Department of Economics and Business Economics

CoRE Center for Research in Energy, Economics, and Markets

Aarhus University, Denmark

December 13, 2024

Abstract

The Global Carbon Budget, maintained by the Global Carbon Project, summarizes Earth's global carbon cycle through four annual time series beginning in 1959: atmospheric CO₂ concentrations, anthropogenic CO₂ emissions, and CO₂ uptake by land and ocean. We analyze these four time series as a multivariate (cointegrated) system. Statistical tests show that the four time series are cointegrated with rank three and identify anthropogenic CO₂ emissions as the single stochastic trend driving the nonstationary dynamics of the system. The three cointegrated relations correspond to the physical relations that the sinks are linearly related to atmospheric concentrations and that the change in concentrations equals emissions minus the combined uptake by land and ocean. Furthermore, likelihood ratio tests show that a parametrically restricted error-correction model that embodies these physical relations and accounts for the El-Niño/Southern Oscillation cannot be rejected on the data. Finally, projections based on this model, using Shared Socioeconomic Pathways scenarios, yield results consistent with established climate science.

*We are grateful to Chris Smith, Sophocles Mavroeidis, and conference participants at EMCC-VIII in Cambridge 2024 as well as at AWE-V in Aarhus 2024 for helpful comments. Nielsen thanks the Danish National Research Foundation for financial support (DNRF Chair grant number DNRF154). Bennedsen thanks the Independent Research Fund Denmark for financial support (IRFD grant number 0219-00001B).

[†]Email: mbennedsen@econ.au.dk

[‡]Corresponding author, email: ehillebrand@econ.au.dk

[§]Email: mon@econ.au.dk

1 Introduction

We present a cointegrated vector autoregressive (CVAR) model (Johansen, 1995, Juselius, 2006) for the primary time series variables in the Global Carbon Budget (GCB) dataset provided by Friedlingstein et al. (2023). This model enables the statistical estimation of critical parameters of the global carbon cycle and the evaluation of their estimation uncertainty. The model integrates atmospheric carbon dioxide (CO_2) concentrations, anthropogenic emissions, and absorption by both the terrestrial biosphere (land sink) and the ocean (ocean sink). Central to the model is the global carbon budget equation: Changes in atmospheric concentrations are equal to the difference of anthropogenic emissions and the sinks uptake. The model describes the sinks as functions of atmospheric CO_2 levels and the El-Niño/Southern Oscillation (ENSO) cycle. The dependence of sinks on atmospheric concentrations together with the budget equation introduce simultaneity in the GCB variables. Emissions are modeled as a random walk with drift. All variables are trending, and the dependence of the sinks on concentrations as well as the budget equation constitute cointegrating relations.

The approach facilitates a data-driven examination of the global carbon cycle through a compact model incorporating both observational data and outputs from various large-scale Earth system models (ESMs). Historical GCB data are used for parameter estimation via maximum likelihood, and parameter uncertainty is assessed through statistical standard errors. Unlike ESMs or small-scale emulators, the CVAR approach quantifies uncertainty. In contrast to earlier statistical studies of the GCB data set, the CVAR framework allows for formal hypothesis tests of the parametric restrictions motivated by the physical relations.

The Global Carbon Project¹ maintains an extensive database of time series variables describing the carbon cycle dynamics, aiding in understanding the transfer of anthropogenically emitted CO_2 to the atmosphere, oceans, and terrestrial biosphere. These data are updated annually and published in the *Global Carbon Budget* reports. Understanding carbon cycle dynamics is crucial for comprehending the overall climate system and climate change (e.g. Canadell et al., 2021).

The GCB data have been utilized for various statistical analyses. One research strand investigates whether the carbon sinks' CO_2 absorption rate, measured by the airborne fraction or sink rate, is constant, as seen in studies like Raupach et al. (2008), Knorr (2009), Le Quéré et al. (2009), Gloor et al. (2010), Raupach et al. (2014), and Bennedsen et al. (2019, 2024). Other research uses the GCB data's residual, termed the budget imbalance, to verify the accuracy of reported CO_2 emissions by individual nations, as discussed in, e.g., Peters et al. (2017) and Bennedsen (2021). Previous statistical analyses of the GCB data often limit model dimensions to univariate or bivariate settings and rarely

¹<https://www.globalcarbonproject.org>.

consider all GCB variables together. Early studies, such as [Enting and Lassey \(1993\)](#) and [Parkinson and Young \(1998\)](#), evaluated parameter uncertainty in global carbon cycle models using statistical methodologies. [Bennedsen et al. \(2023\)](#) specify a comprehensive multivariate dynamic model of the GCB variables in a state space framework.

In this paper, we leverage the advantages of the CVAR framework that allows for specifying an unrestricted multivariate model that is agnostic about the physical relations of the variables and that nests the restricted, physically motivated model as a special case. Then, we conduct a comprehensive (likelihood ratio) hypothesis test for whether the physical restrictions are supported by the data. Since we find that this is the case, we proceed with the restricted model and explore projections of future paths of the global carbon cycle.

The outline of the paper is as follows. In [Section 2](#), we explain the physical relations in the GCB data set and how they motivate a cointegration approach. We specify the restricted, physically motivated model. In [Section 3](#), we specify the unrestricted model by way of standard cointegration and specification tests. We then conduct a likelihood ratio test of the restricted against the unrestricted model, and we find that the data support the restricted, physically motivated model. We report the estimation results for the restricted model and discuss their physical meaning in the context of the system nature of the model. We also present residual diagnostics. In [Section 4](#), we apply the model to explore future projections of the paths of the system using scenarios from the Shared Socioeconomic Pathways (SSP) initiative ([Riahi et al., 2017](#)). [Section 5](#) concludes.

2 Trends and cointegration in the Global Carbon Budget

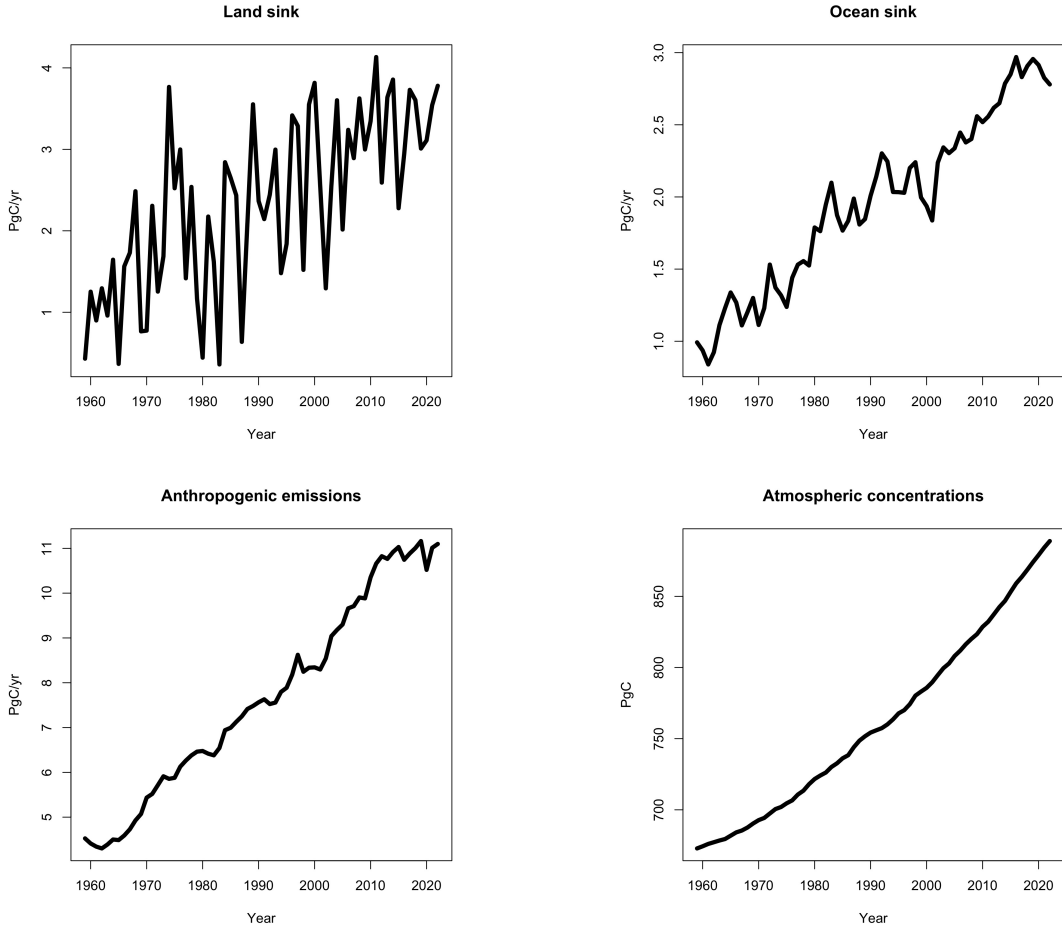
[Figure 1](#) displays the time series data set from the Global Carbon Project studied in this paper. The GCB time series are annual from 1959 to 2022, measured in PgC (per year), and obtained from the global file of [Friedlingstein et al. \(2023\)](#).²

The top left panel in [Figure 1](#) shows the CO₂ uptake by the terrestrial biosphere (land sink), and the top right panel that by the oceans (ocean sink). The bottom left panel shows anthropogenic CO₂ emissions, calculated as the sum of fossil fuel and land-use change emissions minus the cement carbonation sink from the global file of [Friedlingstein et al. \(2023\)](#). The bottom right panel shows the “Keeling curve” of atmospheric CO₂ concentrations.

[Figure 1](#) shows that all time series are upwards trending. The source of trend in the land and ocean sink dynamics are atmospheric concentrations. [Bacastow and Keeling \(1973\)](#) and [Gifford \(1993\)](#) have proposed the most commonly used functions that relate atmospheric CO₂ concentrations and land uptake. [Bacastow and Keeling \(1973\)](#) argue that the linear approximation to their function describes the relation well as long as concentrations do not deviate too far from pre-industrial concentrations. [Bennedsen et al.](#)

²Available at <https://globalcarbonbudgetdata.org>.

Figure 1: GCB annual time series 1959–2022



Notes: PgC is petagram of carbon (division by 2.12 yields ppm).

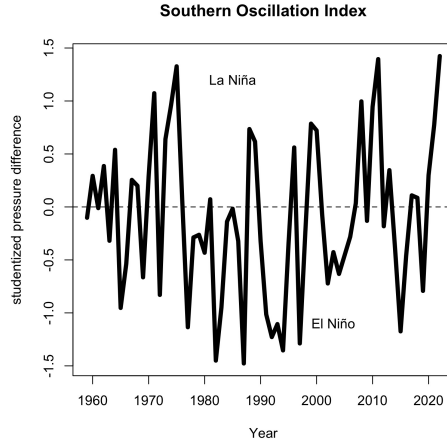
(2023) demonstrate on the GCB data set 1959–2020 that the linear approximation is accurate for both the land and ocean sink. We can therefore specify the sinks equations as

$$\begin{aligned} S_t^L &= a_1 + b_1 C_t + X_{1,t}, \\ S_t^O &= a_2 + b_2 C_t + X_{2,t}, \end{aligned} \tag{1}$$

where S_t^L and S_t^O are land and ocean sink, respectively, and C_t are atmospheric concentrations. The deviations processes $X_{\{1,2\},t} = \phi_{\{1,2\}} X_{\{1,2\},t-1} + \varepsilon_{\{1,2\},t}$, where $\varepsilon_{\{1,2\},t}$ are independent i.i.d. zero-mean variables, are specified as AR(1) time series. If $\phi_{\{1,2\}} = 0$, there is no autocorrelation in the deviations from the trend given by atmospheric concentrations. Univariate unit root tests of the sinks time series identify them as trend-stationary, since atmospheric concentrations follow a near-linear trend, see Figure 1.

ENSO is found to explain some of the variation in the sinks in addition to concentrations (Feely et al., 1999, Haverd et al., 2018, Bennedsen et al., 2023). ENSO is, however, a stationary, if cyclical, phenomenon, while atmospheric concentrations are nonstationary. Concentrations are thus by far the dominant explanatory variable in the sinks and central to the cointegrating relations. In this paper, we use the Southern Oscillation In-

Figure 2: Southern Oscillation Index (SOI) 1959–2022



index (SOI) as a measure of ENSO, see Figure 2. The SOI is the studentized pressure differential between Tahiti and Darwin, Australia. It is obtained from [Climatic Research Unit \(2024\)](#), [Ropelewski and Jones \(1987\)](#). Positive values of the SOI are indicative of a La-Niña phase, negative values of an El-Niño phase.

The land uptake of CO_2 increases during the La-Niña phase of the ENSO due to moisture sensitivity of plants ([Haverd et al., 2018](#)). The ocean uptake is reduced during the La Niña phase due to increased deep upwelling that brings carbon-rich waters to the surface ([Feely et al., 1999](#)). Therefore, we expect the land sink to depend positively on SOI and the ocean sink negatively.

[Bennedsen et al. \(2023\)](#) show that anthropogenic emissions E_t are well described by a random walk with drift $d > 0$:

$$E_t = d + E_{t-1} + X_{3,t}, \quad (2)$$

where $X_{3,t} = \phi_3 X_{3,t-1} + \varepsilon_{3,t}$, $\varepsilon_{3,t}$ i.i.d. zero-mean random variable. Atmospheric concentrations C_t are given by the *global carbon budget equation*:

$$C_t = C_{t-1} + E_t - S_t^L - S_t^O + X_{4,t}, \quad (3)$$

where $X_{4,t} = \phi_4 X_{4,t-1} + \varepsilon_{4,t}$, $\varepsilon_{4,t}$ i.i.d. zero-mean random variable. The budget equation states that changes in atmospheric concentrations, ΔC_t , are given by anthropogenic emissions minus the combined land and ocean uptake plus an error, which corresponds to the *budget imbalance* variable in the global data file of [Friedlingstein et al. \(2023\)](#). The initial value of C_t in 1959 is 670 PgC.

[Bennedsen et al. \(2023\)](#) report comprehensive unit root test results on the data set. The four main variables are all found to be (trend-)stationary I(1) processes. The SOI is found to be stationary. With this in mind, the model equations in (1) and (3) suggest that our system of $p = 4$ variables is nonstationary I(1) and contains three linear cointegrating combinations that are stationary I(0). We model the variables collected in $Y_t =$

$(S_t^L, S_t^O, E_t, C_t)'$ in the vector autoregressive (VAR) framework, and the analysis thus fits perfectly in the cointegrated VAR (CVAR) setup; see [Johansen \(1995\)](#), [Juselius \(2006\)](#).

The CVAR model for a p -dimensional vector time series Y_t is given in vector error-correction model (VECM) form as

$$\Delta Y_t = \mu + \alpha\beta'Y_{t-1} + \sum_{j=1}^k \Gamma_j \Delta Y_{t-j} + \Phi X_t + U_t, \quad (4)$$

where, as usual, the error term U_t is assumed to be p -dimensional independent and identically distributed with mean zero and covariance matrix Σ . The long-run parameters α and β are $p \times r$ matrices with $0 \leq r \leq p$. The rank r is termed the cointegration rank, and the columns of β constitute the r cointegration vectors such that $\beta'Y_t$ are the stationary long-run equilibrium relations. The parameters in α are the adjustment parameters that represent the speed of adjustment towards equilibrium for each of the variables. To allow for a deterministic level (mean in the cointegrating relations) and a linear trend in the variables, we have included a so-called unrestricted constant term, μ . Finally, X_t allows inclusion of exogenous variables, and the short-run dynamics are governed by the autoregressive parameters $\Gamma_1, \dots, \Gamma_k$ with lag-order denoted by k (that is, there are $k+1$ lags in the VAR representation and equivalently k lags in the VECM representation).

The model specified in (1) through (3) can be written in structural VAR form as

$$\begin{aligned} \begin{bmatrix} 1 & 0 & 0 & -b_1 \\ 0 & 1 & 0 & -b_2 \\ 0 & 0 & 1 & 0 \\ 1 & 1 & -1 & 1 \end{bmatrix} \begin{bmatrix} \Delta S_t^L \\ \Delta S_t^O \\ \Delta E_t \\ \Delta C_t \end{bmatrix} &= \begin{bmatrix} a_1(1 - \phi_1) \\ a_2(1 - \phi_2) \\ d(1 - \phi_3) \\ 0 \end{bmatrix} + \begin{bmatrix} b_3 \\ b_4 \\ 0 \\ 0 \end{bmatrix} SOI_t \\ &+ \begin{bmatrix} -(1 - \phi_1) & 0 & 0 & b_1(1 - \phi_1) \\ 0 & -(1 - \phi_2) & 0 & b_2(1 - \phi_2) \\ 0 & 0 & 0 & 0 \\ -(1 - \phi_4) & -(1 - \phi_4) & 1 - \phi_4 & 0 \end{bmatrix} \begin{bmatrix} S_{t-1}^L \\ S_{t-1}^O \\ E_{t-1} \\ C_{t-1} \end{bmatrix} \\ &+ \begin{bmatrix} 0 & 0 & 0 & 0 \\ 0 & 0 & 0 & 0 \\ 0 & 0 & \phi_3 & 0 \\ 0 & 0 & 0 & \phi_4 \end{bmatrix} \begin{bmatrix} \Delta S_{t-1}^L \\ \Delta S_{t-1}^O \\ \Delta E_{t-1} \\ \Delta C_{t-1} \end{bmatrix} + \begin{bmatrix} \varepsilon_{1,t} \\ \varepsilon_{2,t} \\ \varepsilon_{3,t} \\ \varepsilon_{4,t} \end{bmatrix}, \quad (5) \end{aligned}$$

where we have added SOI with coefficient vector $[b_3, b_4, 0, 0]'$, where b_3 and b_4 are unrestricted (expected to be estimated positive respectively negative). Left-multiplying (5) with the inverse of the leading matrix of concurrent relations, we obtain the VECM form

(4) with

$$\begin{aligned}
\mu &= \begin{bmatrix} \frac{a_1}{c}(1-\phi_1)(1+b_2) - \frac{b_1}{c}(a_2(1-\phi_2) - d(1-\phi_3)) \\ \frac{a_2}{c}(1-\phi_2)(1+b_1) - \frac{b_2}{c}(a_1(1-\phi_1) - d(1-\phi_3)) \\ d(1-\phi_3) \\ \frac{1}{c}(d(1-\phi_3) - a_1(1-\phi_1) - a_2(1-\phi_2)) \end{bmatrix}, \\
\alpha &= \begin{bmatrix} -\frac{(1+b_2)(1-\phi_1)}{c} & \frac{b_1(1-\phi_2)}{c} & \frac{b_1(1-\phi_4)}{c} \\ \frac{b_2(1-\phi_1)}{c} & -\frac{(1+b_1)(1-\phi_2)}{c} & \frac{b_2(1-\phi_4)}{c} \\ 0 & 0 & 0 \\ \frac{1-\phi_1}{c} & \frac{1-\phi_2}{c} & \frac{1-\phi_4}{c} \end{bmatrix}, \quad \beta' = \begin{bmatrix} 1 & 0 & 0 & -b_1 \\ 0 & 1 & 0 & -b_2 \\ -1 & -1 & 1 & 0 \end{bmatrix}, \\
\Gamma_1 &= \begin{bmatrix} 0 & 0 & \frac{b_1\phi_3}{c} & \frac{b_1\phi_4}{c} \\ 0 & 0 & \frac{b_2\phi_3}{c} & \frac{b_2\phi_4}{c} \\ 0 & 0 & \phi_3 & 0 \\ 0 & 0 & \frac{\phi_3}{c} & \frac{\phi_4}{c} \end{bmatrix}, \quad \Phi X_t = \begin{bmatrix} \frac{b_3(1+b_2)-b_1b_4}{c} \\ \frac{b_4(1+b_1)-b_2b_3}{c} \\ 0 \\ -\frac{b_3+b_4}{c} \end{bmatrix} SOI_t, \tag{6}
\end{aligned}$$

where $c = 1 + b_1 + b_2$, and the error vector is

$$U_t = \begin{bmatrix} \frac{1+b_2}{c} & \frac{-b_1}{c} & \frac{b_1}{c} & \frac{b_1}{c} \\ \frac{-b_2}{c} & \frac{1+b_1}{c} & \frac{b_2}{c} & \frac{b_2}{c} \\ 0 & 0 & 1 & 0 \\ -\frac{1}{c} & -\frac{1}{c} & \frac{1}{c} & \frac{1}{c} \end{bmatrix} \begin{bmatrix} \varepsilon_{1,t} \\ \varepsilon_{2,t} \\ \varepsilon_{3,t} \\ \varepsilon_{4,t} \end{bmatrix} = \begin{bmatrix} \frac{1+b_2}{c}\varepsilon_{1,t} + \frac{b_1}{c}(-\varepsilon_{2,t} + \varepsilon_{3,t} + \varepsilon_{4,t}) \\ \frac{1+b_1}{c}\varepsilon_{2,t} + \frac{b_2}{c}(-\varepsilon_{1,t} + \varepsilon_{3,t} + \varepsilon_{4,t}) \\ \varepsilon_{3,t} \\ \frac{1}{c}(-\varepsilon_{1,t} - \varepsilon_{2,t} + \varepsilon_{3,t} + \varepsilon_{4,t}) \end{bmatrix}.$$

The model (5) is equivalent to (4) with coefficient matrices (6). The first row of β' shows the cointegrating relation between S^L and C , the second row the cointegrating relation between S^O and C , and the third row the cointegrating relation of the carbon budget equation between S^L , S^O , and E . The adjustment coefficients in α show that S^L , S^O , and C adjust to disequilibrium in all cointegrating relations, whereas E does not adjust at all. This shows the special role of emissions as driver of the system, or, in other words, as the only source of deterministic and stochastic trend. It is apparent that the cointegrating rank is three, and the number of common stochastic trends therefore one, and given by the emissions.

The system (4) has $k = 1$ lagged difference, and the coefficient Γ_1 of the first lag of differences, $Y_{t-1} = (\Delta S_{t-1}^L, \Delta S_{t-1}^O, \Delta E_{t-1}, \Delta C_{t-1})'$, captures the short-run dynamics in stationary first differences of the system variables. It is apparent that autocorrelation in the dynamics of the deviations from the trend in the sinks S^L and S^O , driven by atmospheric concentrations C as captured by the autoregressive coefficients ϕ_1 and ϕ_2 in (1), does not play a role in the short-run dynamics of the cointegrated system. In fact, the first two columns of Γ_1 are zero. The reason can be understood from (5), where accounting for the contemporaneous relation $\Delta S_t^L - b_1 \Delta C_t$ on the left-hand side removes all influence of the serial correlation parameter ϕ_1 from the first differences and fully absorbs it in the dependence on the lagged level S_{t-1}^L . The same holds for S^O .

The global carbon budget equation, as a cointegrating relation, implies an influence of SOI on ΔC , by way of its influence on the sinks. This leads to a non-zero coefficient on SOI in the last row. The error term U_t is a linear combination of the structural errors ε_t , by way of the contemporaneous relations, and the covariance matrix of U_t is, therefore, not diagonal. However, the correlations are purely contemporaneous, and there is no serial correlation.

3 Estimating and testing the model

In this section, we first determine the lag order, and then we find a benchmark model that is unrestricted except in the cointegrating rank, which we determine using the Johansen trace tests. We then test the parameter restrictions (6) implied by the model (5) against the unrestricted model, including exogeneity of emissions and the form of the cointegrating relations. Finally, we report estimation results and residual diagnostics for the restricted model (5).

3.1 Unrestricted benchmark model

The model in (1)–(3) informs our choice of deterministic terms. An unrestricted constant in the VECM, which is defined in first differences ΔY_t , translate into linear trends in levels Y_t , and this is precisely the form of the emissions equation (2). There are no other types of trend in the model, and therefore the only deterministic term is an unrestricted constant.

In analyzing the cointegrating rank in an unrestricted VAR for $Y_t = (S_t^L, S_t^O, E_t, C_t)'$, one can argue for including or excluding SOI as an explanatory variable, in addition to the unrestricted constant. The SOI explains some variation in the system, but as a stationary variable, it is not central to the cointegrating relations, as noted above. Based on residual diagnostics, reported in Table 5 in Appendix A, we note that we need either $k = 1$ lag or inclusion of SOI , or preferably both. For robustness, we report in Table 1 the trace test statistics for all four variations: with and without SOI and with and without a lagged difference.

A priori, we expect three cointegrating relations to be present in Y_t as given by (1) and (3). For the latter we note that E , S^L , and S^O cointegrate in the budget equation with cointegrating vector $(1, -1, -1)$ to yield $\Delta C_t - X_{4,t}$, which is $I(0)$. Equivalently, emissions are the only source of stochastic trend in the system. Table 1 confirms that the clear finding from all four specifications that we consider here, without imposing any restrictions on the parameters, is a rank of three. At this point, the statistics cannot tell whether emissions play any specific role.

We note that including SOI strengthens the significance of the third cointegrating relation. Consequently, our chosen unrestricted benchmark model is the cointegrated VAR with one lagged difference, cointegration rank three, and including SOI and an unrestricted constant term as exogenous explanatory variables. The VECM form of the

Table 1: Trace statistic for cointegrating rank r in system of dimension $p = 4$

r	$p - r$	Eigenvalue	Trace	5% critical	P -value
No SOI, $k = 0$ lags					
0	4	0.8030	157.34	47.71	0.000
1	3	0.4625	55.01	29.80	0.000
2	2	0.2122	15.90	15.41	0.042
3	1	0.0137	0.87	3.84	0.350
With SOI, $k = 0$ lags					
0	4	0.8000	184.86	47.71	0.000
1	3	0.5662	83.47	29.80	0.000
2	2	0.3758	30.85	15.41	0.000
3	1	0.0182	1.16	3.84	0.281
No SOI, $k = 1$ lag					
0	4	0.5185	89.43	47.71	0.000
1	3	0.3680	44.11	29.80	0.000
2	2	0.2114	15.66	15.41	0.046
3	1	0.0151	0.94	3.84	0.332
With SOI, $k = 1$ lag					
0	4	0.5931	110.31	47.71	0.000
1	3	0.4267	54.57	29.80	0.000
2	2	0.2666	20.07	15.41	0.008
3	1	0.0135	0.85	3.84	0.358

benchmark model is thus given by (4) with $p = 4$, $k = 1$, $r = 3$, and $X_t = SOI_t$, where α and β are of dimension $p \times r = 4 \times 3$ and U_t is the 4×1 reduced-form error vector.

Letting \hat{U}_t denote the residuals, the maximized (quasi) log-likelihood function of the model is

$$\begin{aligned} \mathcal{L} &= -\frac{Tp}{2} \log 2\pi - \frac{T}{2} \log \det \hat{\Sigma} - \frac{1}{2} \sum_{t=1}^T \hat{U}_t' \hat{\Sigma}^{-1} \hat{U}_t \\ &= -\frac{Tp}{2} \log 2\pi - \frac{T}{2} \log \det \hat{\Sigma} - \frac{Tp}{2}, \end{aligned} \quad (7)$$

where $T = 63$ is the number of observations of ΔY_t , and

$$\hat{\Sigma} = \frac{1}{T} \sum_{t=1}^T \hat{U}_t \hat{U}_t'$$

is the estimate of the covariance matrix of the reduced-form errors. Our estimated benchmark model has a numerically maximized log-likelihood of -30.217 . Determining the degrees of freedom in the model accounts for the matrix α of dimension $p \times r$, with 12 free parameters, the matrix β of dimension $p \times r$, where the leading $r \times r$ block is restricted to the identity matrix because of the cointegrating relations, leaving $(p - r)r = 3$ free parameters. In addition, there is the intercept vector of dimension p and the short-run coefficient matrix Γ_1 of dimension $p \times p$, which together add 20 free parameters. Finally,

Table 2: LR tests of variable exclusion and weak exogeneity in the unrestricted model (4)

Variable	Exclusion	P -value	Weak exogeneity	P -value
S_t^L	39.961	0.000	46.300	0.000
S_t^O	37.399	0.000	38.291	0.000
E_t	18.432	0.000	0.230	0.973
C_t	4.927	0.177	26.081	0.000

Notes: All LR test statistics are asymptotically χ^2 -distributed with three degrees of freedom. The null hypothesis of the exclusion test is a row of zeros in β . The null hypothesis of the weak exogeneity test is a row of zeros in α .

the p -dimensional coefficient vector on SOI adds 4 free parameters, for a total of 39 free parameters.

3.2 Testing the restrictions

We first test for weak exogeneity and variable exclusion. Testing for weak exogeneity of each variable means testing whether the corresponding row in the α matrix is zero. In the latter case, the variable does not adjust to disequilibrium in any of the cointegrating relations. This could be either because it is not a relevant variable for the system or because it is a driver of the system. If the variable is not relevant for the cointegrating relations, then the corresponding row in the β matrix is zero, i.e., variable exclusion. In particular, if a variable is relevant and cannot be excluded, in addition to its α row being zero, then it is causing disequilibrium without adjusting to it, and it is therefore a driver of the system.

Table 2 shows the results of LR tests for zero rows in β (exclusion) and α (weak exogeneity). The test for exclusion shows that emissions E cannot be excluded from the cointegrating relations in the unrestricted model (4), so emissions are important to explain the system dynamics. At the same time, the row in α corresponding to emissions is not distinguishable from zero (weak exogeneity), and therefore emissions do not adjust to disequilibrium. No other variable plays a similar role, so we conclude that emissions are the central driver of the system.

We also note that we cannot reject exclusion of atmospheric concentrations C in the reduced-form unrestricted model with an unrestricted constant term. However, including an unrestricted constant term for ΔS_t^L and ΔS_t^O results in linear deterministic trends in the sinks. Thus, allowing for linear deterministic trends in the sinks masks the necessity of C in explaining the dynamics and the trends in the sinks. This shows the importance of imposing parameter restrictions for capturing basic physical relations. Specifically, in the structural model (5), the intercept vector and coefficients $\Pi = \alpha\beta'$ and Γ_1 in (6) are such that model (5) does not allow for linear deterministic trends in the sinks, but C must be used to explain the trending behavior of the sinks.

Table 3: Maximum likelihood estimates of the parameters in model (5)

Parameter	Estimate	Standard error
a_1	-5.0392	1.1134
a_2	-4.8127	0.2860
b_1	0.0098	0.0014
b_2	0.0089	0.0004
b_3	0.5723	0.1121
b_4	-0.1086	0.0174
d	0.1076	0.0213
ϕ_1	0.0923	0.1066
ϕ_2	0.4841	0.0834
ϕ_3	-0.1169	0.1259
ϕ_4	0.2810	0.1216

The restricted, structural model (5) has the parameter vector

$$\theta = (a_1, a_2, b_1, b_2, b_3, b_4, d, \phi_1, \phi_2, \phi_3, \phi_4,)',$$

which is of dimension 11. The log-likelihood can be evaluated using (7), as in the unrestricted model. Model (5) is restricted in the system matrices (6) in the VECM, that is, in the way the residuals \hat{U}_t are computed. The numerically maximized log-likelihood of model (5) is -45.908 . Testing the restricted specification (5) against the unrestricted (4) therefore amounts to evaluating the LR test statistic

$$LR = -2(-45.908 - (-30.217)) = 31.382,$$

which is asymptotically χ^2 -distributed with $39 - 11 = 28$ degrees of freedom. The P -value is 0.30, and the restricted model cannot be rejected by the data on the sample period at any standard significance level. We therefore adopt the restricted, structural model (5) as our preferred model.

3.3 Estimation of the restricted model

Table 3 reports maximum likelihood estimates of the parameters of model (5) together with standard errors. The unit of measurement of the sinks S (for both $S = S^L$ and $S = S^O$) is PgC and linear in atmospheric concentrations C in excess of pre-industrial levels, i.e., $S \approx b(C - C_{1750})$. The magnitude of the intercepts is, thus, approximately $a \approx -bC_{1750}$, where the 1750-level atmospheric concentrations are 593 PgC, or about 280 ppm.

The trend parameters of the sinks relative to atmospheric concentrations are very similar, and they compare with those found in Bennedsen et al. (2023). The global carbon budget equation (3) states that $C_t - C_{t-1} = E_t - S_t^L - S_t^O + X_t$, where $X_t = X_{4,t} - X_{1,t} - X_{2,t}$ is a stationary error. As a consequence of (1),

$$(1 + b_1 + b_2)C_t - C_{t-1} = E_t - (a_1 + a_2) + X_t,$$

which shows that the dynamics of atmospheric concentrations C_t are determined by the

stochastic trend in emissions E_t , which propagates in time according to the autoregressive lag polynomial $\Phi(L) = 1 - (1 + b_1 + b_2)^{-1}L$. The sum $b_1 + b_2$ keeps the dynamics of C_t from a second unit root, in addition to the one in emissions. If the sinks saturate (Canadell et al., 2007, Le Quéré et al., 2007) and the coefficients b_1 and b_2 decrease, the dynamics of C_t approach $I(2)$.

The deviations of the sinks from their trends have different dynamics, as can be seen in Figure 1. The trend deviations of the land sink are of higher variance with no visually discernible serial correlation, whereas the deviations of the ocean sink are tighter around the trend with more apparent patterns of serial correlation. This is supported by the estimates of the AR(1) parameters ϕ_1 (indistinguishable from zero) and ϕ_2 (significantly positive).

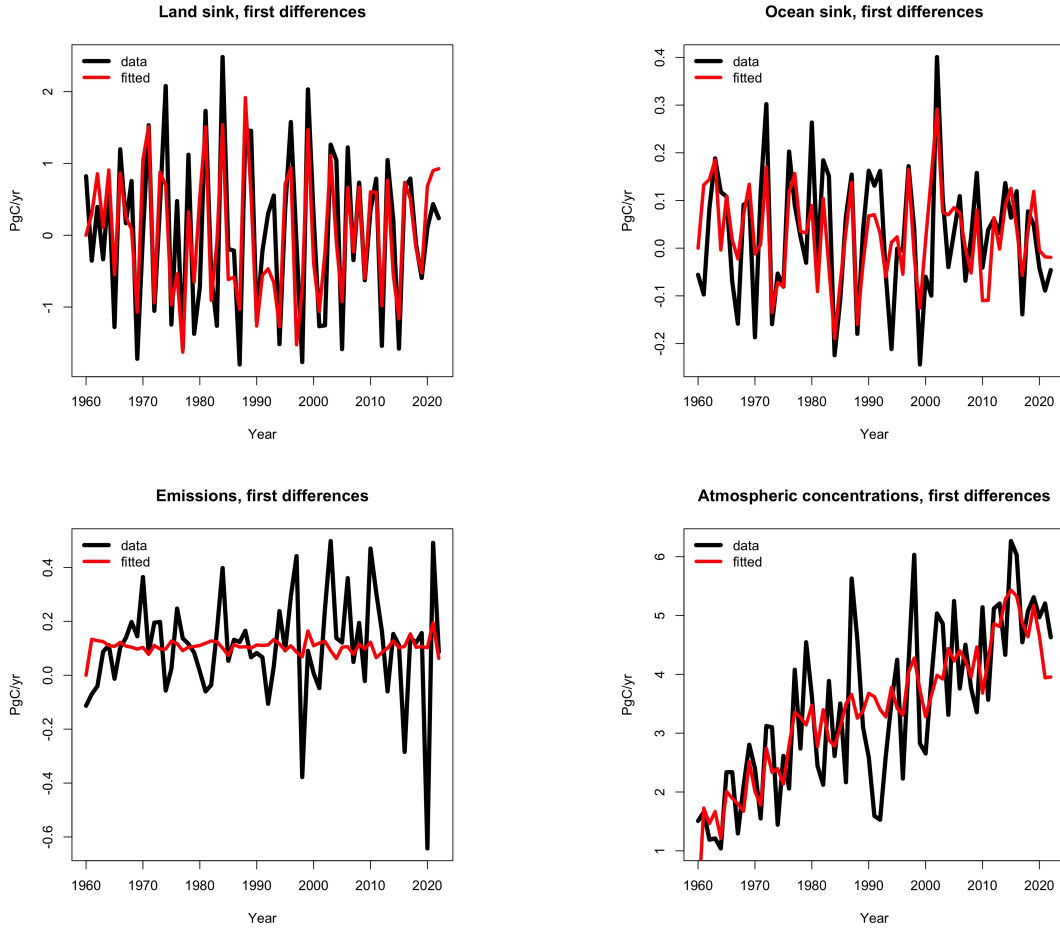
The serial correlation in first differences of emissions (ϕ_3) is indistinguishable from zero, whereas the error in the budget equation has mild serial correlation (ϕ_4). The drift d in emissions is in line with estimates reported earlier (Bennedsen et al., 2023). The coefficients b_3 and b_4 on SOI in the sinks have the expected sign and are significantly different from zero.

Figure 3 shows the fit of model (5) to the data of first differences of the system variables. It can be seen that the model captures variations in the sinks very well. A random walk with drift is a simple model that captures the main role of emissions as driver of the system and source of deterministic and stochastic trend in the cointegrating relations. The lower left panel of Figure 3 shows that there is room for improvement in capturing short-run fluctuations of first-differenced emissions, but this is beyond the scope of this paper. In order to explain short-run fluctuations in emissions, macroeconomic data have to be included in the analysis (Bennedsen et al., 2021).

Figure 3 shows that first differences of atmospheric concentrations are upward trending, i.e., that the average annual increase in atmospheric concentrations is rising. In the cointegration analysis of the unrestricted model (4), there is an unrestricted intercept for ΔC , and thus an unrestricted linear trend for C . This removes all trending behavior from ΔC . In the restricted model (5), in contrast, ΔC is given by the budget equation as $\Delta C = \Delta E - \Delta S^L - \Delta S^O$. First differences in emissions have an unrestricted intercept d , implying an unrestricted trend dt in E . The sinks have trends that are linear functions of atmospheric concentrations C . Due to the nearly linear behavior of C (Figure 1), these trends can be approximated by linear trends with slopes implied by the free parameters b_1 and b_2 ; see (6). The resulting trend in ΔC , which is the trend in emissions minus the trends in the sinks, is not equal to zero, and first differences of atmospheric concentrations appear trend-stationary. Again, the parametric restrictions are important in capturing this important property of the data.

Table 4 shows the residual diagnostics for model (5). The only tests that reject are the Ljung-Box test (up to lag 10) for autocorrelation in the residuals of the land sink equation

Figure 3: First differences of the system variables and fit of model (5)



Notes: PgC is petagram of carbon (division by 2.12 yields ppm).

Table 4: Residual diagnostics for the restricted model (5)

Variable	Std Dev	Skew	Kurt	JB	LB(5)	LB(10)
ΔS_t^L	0.651	0.204	2.352	0.471	0.339	0.008
ΔS_t^O	0.094	-0.446	3.163	0.312	0.972	0.989
ΔE_t	0.187	-0.851	6.199	0.000	0.510	0.468
ΔC_t	0.656	-0.146	2.276	0.485	0.943	0.117
System				0.015	0.980	0.707

Notes: System denotes system-wide (vector) tests. Std Dev: standard deviation, Skew: skewness, Kurt: kurtosis, JB: P -value of Jarque-Bera test for normality, LB(j): P -value of Ljung-Box test for serial correlation up to lag j .

and the Jarque-Bera test for Gaussianity of the residuals in the emissions equation. The latter is due to non-zero skewness and excess kurtosis and could likely be remedied by adding dummy variables for events such as Covid-19 in the emissions equation. The former, if it is not spurious, hints at dynamics in the land sink at the decadal time scale. Since the time series studied here are rather short ($T = 63$), we do not attempt to model these potential dynamics here.

4 Projections

In this section, we apply the estimated restricted model to construct out-of-sample projections of the climate variables C_t , S_t^L , and S_t^O , conditional on a path for the exogenous emissions variable E_t , over the period 2023–2100. In Section 4.1, we discuss the exogenous emissions data used for the projections, Section 4.2 lays out the projection methodology, and Section 4.3 presents the projection results.

4.1 Out-of-sample emissions data

We consider emissions trajectories implied by the Shared Socioeconomic Pathways (SSPs; Riahi et al., 2017), as generated by the climate model MAGICC (Meinshausen et al., 2011).³ These trajectories are hypothesized pathways of future atmospheric CO₂ emissions extensively used in the sixth Assessment Report of the United Nations’ Intergovernmental Panel of Climate Change (IPCC). SSP scenarios are labeled as “SSPX-Y”, where “X” specifies a certain socioeconomic “narrative” used in the construction of the scenario, while “Y” describes the level of radiative forcing (given in W/m²) implied by the scenario in the year 2100.⁴ For instance, SSP1-1.9 refers to the SSP scenario in narrative 1, consistent with 1.9 W/m² of radiative forcing in the year 2100 above pre-industrial levels. Here we do not focus on the various narratives, but only wish to select a number of emission trajectories that represent a range of possible future emissions pathways. We therefore select five “canonical” SSP scenarios, SSP1-1.9, SSP4-3.4, SSP2-4.5, SSP3-3.7, and SSP5-8.5, as exogenous input into our projections (O’Neill et al., 2016). These are shown in the left-most panels in Figure 4. We refer to Riahi et al. (2017) for further details on the SSP scenarios.

4.2 Projection methodology

Given an exogenous emissions scenario E_t^* for $t = 2023, 2024, \dots, 2100$, we form the sequence

$$d_t = E_t^* - E_{t-1}^*,$$

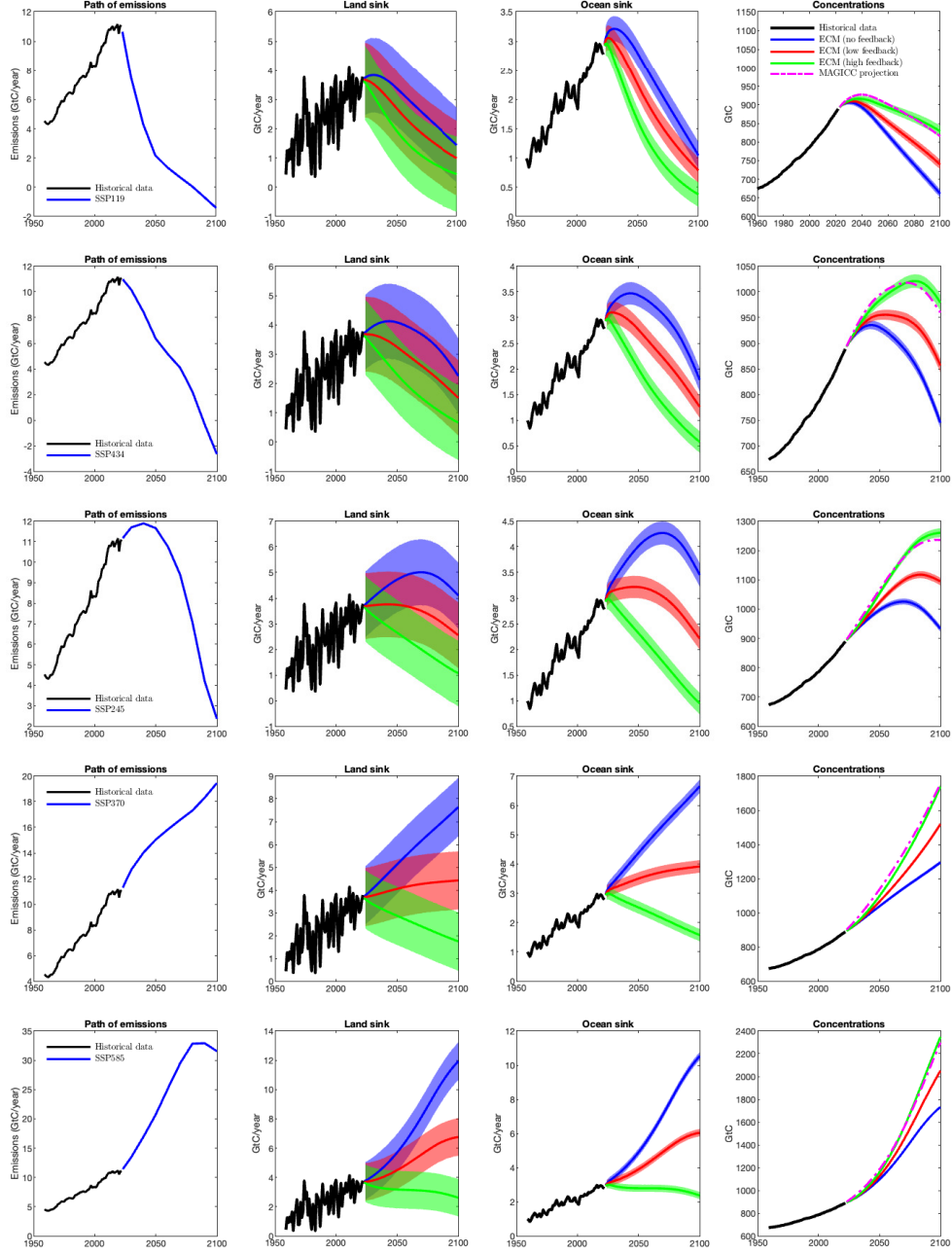
where $E_{2022}^* = E_{2022} = 11.0980$ is set equal to the last in-sample value of the emissions from the GCB data set. The sequence d_t is used as a time-varying drift parameter in the emission equation of our restricted model and serves to ensure that the model-implied emissions are equal to those of the SSP scenario in the out-of-sample period. In particular, for $t \geq 2023$, we modify (2) as follows

$$E_t = d_t + E_{t-1}, \tag{8}$$

³The MAGICC climate model can be run in a browser at <https://live.magicc.org/>.

⁴The conversion from emissions pathway to a forcing level in 2100 is done using climate models, see O’Neill et al. (2016) for details.

Figure 4: Projections of the climate variables under five SSP scenarios



Notes: The five rows correspond to SSP scenarios 119, 434, 245, 370, and 585, respectively. Black: Historical (1959-2022) data. The first column is the CO₂ emissions series used as input. Remaining columns present the simulated climate output variables for three different magnitudes of climate feedback, with shaded areas denoting simulated 97.5% and 2.5% point wise quantiles, and the solid line denoting 50% point wise quantiles. Number of simulations: 100,000. Magenta line in right-most column: Projection of atmospheric CO₂ concentrations as output from the MAGICC climate model.

which, using that $d_t = E_t^* - E_{t-1}^*$, can also be written as

$$E_t = E_{2022} + \sum_{\tau=2023}^t d_\tau = E_{2022} + \sum_{\tau=2023}^t (E_\tau^* - E_{\tau-1}^*) = E_t^*,$$

showing that using the time-varying drift d_t and shutting down the disturbance term in the emissions equation (2), means that the model-implied emissions E_t align with the input SSP trajectory E_t^* , $t = 2023, 2024, \dots, 2100$.

The sinks specifications (1) for the restricted model assume that sinks are linear in concentrations. While this assumption is appropriate for the in-sample period (Bennedsen et al., 2023), it may not be an accurate assumption for the out-of-sample period 2023–2100. The reason is that climate change may modify the future sinks/concentration relationship, a phenomenon known as the *climate feedback effect* (e.g. Friedlingstein, 2015). Climate feedback effects mean that the sinks likely take up less CO₂ over 2023–2100 than the linear model (1) would suggest. To capture these feedback effects on the sinks during the out-of-sample period, for $t \geq 2023$ we modify (1) as

$$\begin{aligned} S_t^L &= a_{1,t} + b_{1,t}C_t + X_{1,t}, \\ S_t^O &= a_{2,t} + b_{2,t}C_t + X_{2,t}, \end{aligned} \tag{9}$$

where, for $j = 1, 2$ and $t \geq 2023$,

$$\begin{aligned} a_{j,t} &= \hat{a}_j \cdot \exp(-\gamma_j \cdot (t - 2022)), \\ b_{j,t} &= \hat{b}_j \cdot \exp(-\gamma_j \cdot (t - 2022)), \end{aligned} \tag{10}$$

where $\hat{a}_1 = -5.0392$, $\hat{a}_2 = -4.8127$, $\hat{b}_1 = 0.0098$, $\hat{b}_2 = 0.0089$ are the estimates of $a_{\{1,2\}}$, $b_{\{1,2\}}$ obtained from the in-sample period 1959–2022, see Table 3. The parameters $\gamma_{\{1,2\}} \in \mathbb{R}$ determine the degree of feedback in the land and ocean sink, respectively. When $\gamma_{\{1,2\}} > 0$, the activity of the sinks, as a response to the level of concentrations, weakens as t increases. We note that it is possible that $S_t^{\{L,O\}} < 0$ for some $t \geq 2023$, which would correspond to the carbon sink becoming a carbon source.

There appears to be no consensus in the climate literature on exactly how climate feedback effects modify the sink/concentration relationship in the future. Here, we parametrize the feedback effect parameters $\gamma_{\{1,2\}}$ by

$$\gamma_{\{1,2\}} = \gamma(p_{\{1,2\}}) = -\frac{\log(1 - p_{\{1,2\}})}{28},$$

where $p_{\{1,2\}} \in [0, 1]$ denote the relative degree of weakening of the sinks by mid-century, i.e. 28 years after 2022. For instance, $p_1 = 50\%$ would correspond to the case where the land sink activity in 2050 is half of what it would have been in the absence of feedback effects. We consider three different magnitudes of feedback effects specified by $(p_1, p_2) = (0, 0)$, $(p_1, p_2) = (25\%, 25\%)$, and $(p_1, p_2) = (50\%, 50\%)$. We refer to the first specification as “no feedback”, the second as “low feedback”, and the third as “high feedback”. No feedback specification corresponds to a situation where the sink parameters $a_{\{1,2\},t}$, $b_{\{1,2\},t}$ are held constantly equal to the values estimated on the in-sample data, whereas low (high) feedback corresponds to a situation where both the land and ocean sinks have weakened by 25% (50%) in 2050.

Using a given SSP scenario for emissions, and substituting (8) and (9) for (2) and (1),

respectively, we simulate from the estimated restricted model to generate out-of-sample projections of the climate variables over the period 2023–2100. We generate 100,000 trajectories from the model and report the 2.5%, 50%, and 97.5% pointwise quantiles.

4.3 Projection results

The first column of Figure 4 shows the exogenous input emissions trajectories for the five SSP scenarios. The second to fourth columns of Figure 4 present the projected climate variables for these scenarios, derived using the methodology outlined above. The projected CO₂ concentrations presented in the right-most column are of particular interest, as they translate into global temperature changes.

The emissions exhibit substantial variation across scenarios, and the differences directly influence the projected climate outputs. Additionally, the projections vary significantly depending on the degree of climate feedback incorporated. Notably, in the absence of feedback (blue projections), the sinks continue absorbing CO₂ according to (1), resulting in substantially lower CO₂ concentrations compared to cases with climate feedbacks included.

The magenta dashed lines in the last column of Figure 4 represent the concentration pathway projected by the MAGICC climate model. These projections align closely with those from the high feedback specification of our restricted model. This alignment is significant for two reasons. First, despite the more complex equations used in MAGICC, our model produces comparable results, underscoring its capability to replicate projections from detailed climate models. Second, this similarity arises only under the high feedback specification, where both sinks weaken by $p_1 = p_2 = 50\%$ in 2050. This suggests that consistency with the historical data record, on which our model is estimated, requires large climate feedback effects to materialize between 2023 and 2100.

For context, the third IPCC Assessment Report estimated mid-century feedback effects between 21%–43% for the land sink and 6%–25% for the ocean sink (Prentice et al., 2001). However, more recent studies indicate these estimates may be conservative, underestimating the potential magnitude of future feedback effects (Friedlingstein, 2015).

5 Conclusions

In this paper, we have specified a cointegrated vector autoregressive (CVAR) model for the global variables in the Global Carbon Budget data set. In contrast to earlier comprehensive statistical models of the GCB data, the CVAR approach allows for formal hypothesis tests of the physically motivated functional forms of the land and ocean sinks, the emission dynamics, and the budget equation. The global carbon budget equation and the dependence of the sinks on atmospheric CO₂ concentrations imply simultaneous relations between the variables, and they constitute cointegrating relations at the same time. We specified both a restricted and physically motivated model as well as an unrestricted

and physically agnostic model that nests the restricted model as a special case. A likelihood ratio test showed that the physically motivated, restricted model is supported by the data. We discussed the estimation results in light of the system nature of the variables. We then used the restricted model to explore future projections of the path of the global carbon cycle using SSP scenarios. Recent discussion in the literature (Canadell et al., 2007, Le Quéré et al., 2007) has suggested possible (partial) saturation in the land and ocean sinks in the near future. In the context of our modeling framework, this would constitute a nonlinear, time-dependent cointegrating relationship. Analyzing the GCB data in a model that allows for time-dependence and nonlinearity in the relation between the sinks and atmospheric concentrations is an interesting topic for future research.

References

- Bacastow, R. and Keeling, C. D. (1973). Atmospheric carbon dioxide and radiocarbon in the natural cycle: II. changes from A. D. 1700 to 2070 as deduced from a geochemical model. In *Carbon and the Biosphere Conference Proceedings*, pages 86–135. Brookhaven Symposia in Biology, Upton, New York, USA.
- Bennedsen, M. (2021). Designing a statistical procedure for monitoring global carbon dioxide emissions. *Climatic Change*, 166(21):1–19.
- Bennedsen, M., Hillebrand, E., and Koopman, S. J. (2019). Trend analysis of the airborne fraction and sink rate of anthropogenically released CO₂. *Biogeosciences*, 16(18):3651–3663.
- Bennedsen, M., Hillebrand, E., and Koopman, S. J. (2021). Modeling, forecasting, and nowcasting U.S. CO₂ emissions using many macroeconomic predictors. *Energy Economics*, 96:105118.
- Bennedsen, M., Hillebrand, E., and Koopman, S. J. (2023). A multivariate dynamic statistical model of the global carbon budget 1959—2020. *Journal of the Royal Statistical Society Series A: Statistics in Society*, 186(1):20–42.
- Bennedsen, M., Hillebrand, E., and Koopman, S. J. (2024). A regression-based approach to the CO₂ airborne fraction. *Nature Communications*, 15(8507):1–9.
- Canadell, J.G., Monteiro, P., Costa, M., da Cunha, L. C., Cox, P., Eliseev, A., Henson, S., Ishii, M., Jaccard, S., Koven, C., Lohila, A., Patra, P., Piao, S., Rogelj, J., Syampungani, S., Zaehle, S., and Zickfeld, K. (2021). Global carbon and other biogeochemical cycles and feedbacks. In Masson-Delmotte, V. et al., editors, *Climate Change 2021: The Physical Science Basis. Contribution of Working Group I to the Sixth Assessment Report of the Intergovernmental Panel on Climate Change*. Cambridge University Press.
- Canadell, J. G., Pataki, D. E., Gifford, R., Houghton, R. A., Luo, Y., Raupach, M. R., Smith, P., and Steffen, W. (2007). Saturation of the terrestrial carbon sink. In Canadell, J. G., Pataki, D. E., and Pitelka, L. F., editors, *Terrestrial Ecosystems in a Changing World*, pages 59–78. Springer Berlin Heidelberg, Berlin, Heidelberg.
- Climatic Research Unit (2024). University of East Anglia. Southern Oscillation Index. <https://crudata.uea.ac.uk/cru/data/soi/>. Accessed: 2024-01-15.
- Enting, I. and Lassey, K. (1993). Projections of Future CO₂. CSIRO Division of Atmospheric Research Technical Paper no. 27, http://www.cmar.csiro.au/e-print/open/enting_2000e.pdf.
- Feely, R. A., Wanninkhof, R., Takahashi, T., and Tans, P. (1999). Influence of El Niño on the equatorial Pacific contribution to atmospheric CO₂ accumulation. *Nature*, 398(6728):597–601.
- Friedlingstein, P. (2015). Carbon cycle feedbacks and future climate change. *Philosophical Transactions of the Royal Society A*, 373:20140421.

- Friedlingstein, P., O’Sullivan, M., Jones, M. W., Andrew, R. M., Bakker, D. C. E., Hauck, J., Landschützer, P., Le Quéré, C., Luijkx, I. T., Peters, G. P., Peters, W., Pongratz, J., Schwingshackl, C., Sitch, S., Canadell, J. G., Ciais, P., Jackson, R. B., Alin, S. R., Anthoni, P., Barbero, L., Bates, N. R., Becker, M., Bellouin, N., Decharme, B., Bopp, L., Brasika, I. B. M., Cadule, P., Chamberlain, M. A., Chandra, N., Chau, T.-T.-T., Chevallier, F., Chini, L. P., Cronin, M., Dou, X., Enyo, K., Evans, W., Falk, S., Feely, R. A., Feng, L., Ford, D. J., Gasser, T., Ghattas, J., Gkritzalis, T., Grassi, G., Gregor, L., Gruber, N., Gürses, O., Harris, I., Hefner, M., Heinke, J., Houghton, R. A., Hurtt, G. C., Iida, Y., Ilyina, T., Jacobson, A. R., Jain, A., Jarníková, T., Jersild, A., Jiang, F., Jin, Z., Joos, F., Kato, E., Keeling, R. F., Kennedy, D., Klein Goldewijk, K., Knauer, J., Korsbakken, J. I., Körtzinger, A., Lan, X., Lefèvre, N., Li, H., Liu, J., Liu, Z., Ma, L., Marland, G., Mayot, N., McGuire, P. C., McKinley, G. A., Meyer, G., Morgan, E. J., Munro, D. R., Nakaoka, S.-I., Niwa, Y., O’Brien, K. M., Olsen, A., Omar, A. M., Ono, T., Paulsen, M., Pierrot, D., Pocock, K., Poulter, B., Powis, C. M., Rehder, G., Resplandy, L., Robertson, E., Rödenbeck, C., Rosan, T. M., Schwinger, J., Séférian, R., Smallman, T. L., Smith, S. M., Sospedra-Alfonso, R., Sun, Q., Sutton, A. J., Sweeney, C., Takao, S., Tans, P. P., Tian, H., Tilbrook, B., Tsujino, H., Tubiello, F., van der Werf, G. R., van Ooijen, E., Wanninkhof, R., Watanabe, M., Wimart-Rousseau, C., Yang, D., Yang, X., Yuan, W., Yue, X., Zaehle, S., Zeng, J., and Zheng, B. (2023). Global carbon budget 2023. *Earth System Science Data*, 15(12):5301–5369.
- Gifford, R. (1993). Implications of CO₂ effects on vegetation for the global carbon budget. In Heimann, M., editor, *The Global Carbon Cycle*, pages 159–199. Springer.
- Gloor, M., Sarmienti, J. L., and Gruber, N. (2010). What can be learned about carbon cycle climate feedbacks from the CO₂ airborne fraction? *Atmospheric Chemistry and Physics*, 10:7739–7751.
- Haverd, V., Smith, B., Nieradzick, L., Briggs, P., Woodgate, W., Trudinger, C., Canadell, J., and Cuntz, M. (2018). A new version of the CABLE land surface model (subversion revision r4601) incorporating land use and land cover change, woody vegetation demography, and a novel optimisation-based approach to plant coordination of photosynthesis. *Geoscientific Model Development*, 11:2995–3026.
- Johansen, S. (1995). *Likelihood-Based Inference in Cointegrated Vector Autoregressive Models*. Oxford University Press.
- Juselius, K. (2006). *The Cointegrated VAR Model: Methodology and Applications*. Oxford University Press.
- Knorr, W. (2009). Is the airborne fraction of anthropogenic CO₂ emissions increasing? *Geophysical Research Letters*, 36.
- Le Quéré, C., Raupach, M., Canadell, J., Marland, G., Bopp, L., Ciais, P., Conway, T., Doney, S., Feely, R., Foster, P., Friedlingstein, P., Gurney, K., Houghton, R., House, J., Huntingford, C., Levy, P., Lomas, M., Majkut, J., Metzl, N., Ometto, J., Peters, G., Prentice, I., Randerson, J., Running, S., Sarmiento, J., Schuster, U., Sitch, S., Takahashi, T., Viovy, N., van der Werf, G., and Woodward, F. (2009). Trends in the sources and sinks of carbon dioxide. *Nature Geoscience*, 2:831–836.
- Le Quéré, C., Rödenbeck, C., Buitenhuis, E. T., Conway, T. J., Langenfelds, R., Gomez, A., Labuschagne, C., Ramonet, M., Nakazawa, T., Metzl, N., Gillett, N., and Heimann, M. (2007). Saturation of the southern ocean CO₂ sink due to recent climate change. *Science*, 316(5832):1735–1738.
- Meinshausen, M., Raper, S. C. B., and Wigley, T. M. L. (2011). Emulating coupled atmosphere-ocean and carbon cycle models with a simpler model, MAGICC6 – Part 1: Model description and calibration. *Atmospheric Chemistry and Physics*, 11(4):1417–1456.
- O’Neill, B. C., Tebaldi, C., van Vuuren, D. P., Eyring, V., Friedlingstein, P., Hurtt, G., Knutti, R., Kriegler, E., Lamarque, J.-F., Lowe, J., Meehl, G. A., Moss, R., Riahi, K., and Sanderson, B. M. (2016). The scenario model intercomparison project (ScenarioMIP) for CMIP6. *Geoscientific Model Development*, 9(9):3461–3482.
- Parkinson, S. and Young, P. (1998). Uncertainty and sensitivity in global carbon cycle modeling. *Climate*

Research, 9:157–174.

- Peters, G. P., Le Quéré, C., Andrew, R. M., Canadell, J. G., Friedlingstein, P., Ilyina, T., Jackson, R. B., Joos, F., Korsbakken, J. I., McKinley, G. A., Sitch, S., and Tans, P. (2017). Towards real-time verification of CO₂ emissions. *Nature Climate Change*, 7(12):848–850.
- Prentice, I., Farquhar, G., Fasham, M., Goulden, M., Heimann, M., Jaramillo, V., Kheshgi, H., Le Quéré, C., Scholes, R., and Wallace, D. (2001). The carbon cycle and atmospheric carbon dioxide. In *Climate Change 2001: The Scientific Basis Contribution of Working Group I to the Third Assessment Report of the Intergovernmental Panel on Climate Change*. Cambridge University Press.
- Raupach, M. R., Canadell, J. G., and Quéré, C. L. (2008). Anthropogenic and biophysical contributions to increasing atmospheric CO₂ growth rate and airborne fraction. *Biogeosciences*, 5:1601–1613.
- Raupach, M. R., Gloor, M., Sarmiento, J. L., Canadell, J. G., Frölicher, T. L., Gasser, T., Houghton, R. A., Le Quéré, C., and Trudinger, C. M. (2014). The declining uptake rate of atmospheric CO₂ by land and ocean sinks. *Biogeosciences*, 11(13):3453–3475.
- Riahi, K., van Vuuren, D. P., Kriegler, E., Edmonds, J., O’Neill, B. C., Fujimori, S., Bauer, N., Calvin, K., Dellink, R., Fricko, O., Lutz, W., Popp, A., Cuaresma, J. C., KC, S., Leimbach, M., Jiang, L., Kram, T., Rao, S., Emmerling, J., Ebi, K., Hasegawa, T., Havlik, P., Humpenöder, F., Da Silva, L. A., Smith, S., Stehfest, E., Bosetti, V., Eom, J., Gernaat, D., Masui, T., Rogelj, J., Strefler, J., Drouet, L., Krey, V., Luderer, G., Harmsen, M., Takahashi, K., Baumstark, L., Doelman, J. C., Kainuma, M., Klimont, Z., Marangoni, G., Lotze-Campen, H., Obersteiner, M., Tabeau, A., and Tavoni, M. (2017). The Shared Socioeconomic Pathways and their energy, land use, and greenhouse gas emissions implications: An overview. *Global Environmental Change*, 42:153–168.
- Ropelewski, C. and Jones, P. (1987). An extension of the Tahiti-Darwin southern oscillation index. *Monthly Weather Review*, 115:2161–2165.

A Supplementary empirical results

Table 5: Residual diagnostics for unrestricted VARs

Variable	Std Dev	Skew	Kurt	JB	LB(5)	LB(10)
No SOI, $k = 0$ lags						
S_t^L	0.751	-0.096	2.684	0.943	0.011	0.000
S_t^O	0.116	0.220	2.510	0.603	0.343	0.528
E_t	0.187	-0.901	6.408	0.000	0.665	0.461
C_t	0.894	0.165	2.797	0.837	0.847	0.308
System				0.023	0.837	0.494
With SOI, $k = 0$ lags						
S_t^L	0.617	0.050	2.712	0.983	0.207	0.009
S_t^O	0.087	-0.285	3.161	0.498	0.556	0.848
E_t	0.188	-0.859	6.347	0.000	0.575	0.418
C_t	0.858	-0.082	3.236	0.524	0.973	0.544
System				0.008	0.956	0.663
No SOI, $k = 1$ lag						
S_t^L	0.681	-0.310	2.773	0.546	0.385	0.045
S_t^O	0.108	0.112	2.964	0.794	0.996	0.999
E_t	0.185	-0.941	6.404	0.000	0.573	0.601
C_t	0.843	-0.006	3.158	0.615	0.695	0.261
System				0.029	0.998	0.973
With SOI, $k = 1$ lag						
S_t^L	0.586	0.138	2.805	0.873	0.781	0.376
S_t^O	0.085	-0.410	3.530	0.235	0.905	0.911
E_t	0.185	-0.984	6.540	0.000	0.552	0.636
C_t	0.814	-0.179	3.303	0.440	0.665	0.262
System				0.007	0.995	0.924

Notes: System denotes system-wide (vector) tests. Std Dev: standard deviation, Skew: skewness, Kurt: kurtosis, JB: P -value of Jarque-Bera test for normality, LB(j): P -value of Ljung-Box test for serial correlation up to lag j . Finally, the P -value of LR test of significance of the coefficient Γ_1 in the models with $k = 1$ are 0.057 (no SOI) and 0.399 (with SOI).

Table 5 shows residual diagnostics from estimating unrestricted VARs (in VECM form with unrestricted constants) for four different configurations of lags and SOI. The rows labelled 'System' show system-wide (vector) tests. The columns for the Jarque-Bera tests for normality, the Ljung-Box tests for serial correlation, and the significance tests on Γ_1 show P -values. Without SOI and without lagged differences, there is evidence of serial correlation in the equation for S^L . Adding either $k = 1$ lag or adding SOI weakens the significance of serial correlation, whereas adding SOI *and* $k = 1$ lag removes it convincingly. The column for the Jarque-Bera test shows that the residuals of the emissions equation cannot pass a test for normality due to high kurtosis and negative skew. This can be remedied by adding dummies, for example for the Covid-19 year 2020,

but we do not do this here for the sake of parsimony. Given that all other equations pass the Jarque-Bera test, we accept the leptokurtosis of the emission residuals.